nature chemical biology

ARTICLE

PUBLISHED ONLINE: 8 MAY 2011 | DOI: 10.1038/NCHEMBIO.561

Single-molecule analysis reveals three phases of DNA degradation by an exonuclease

Gwangrog Lee[1,2], Jungmin Yoo[1], Benjamin J Leslie[1,2] & Taekjip Ha[1,2]*

λ exonuclease degrades one strand of duplex DNA in the 5′-to-3′ direction to generate a 3′ overhang required for recombination. Its ability to hydrolyze thousands of nucleotides processively is attributed to its ring structure, and most studies have focused on the processive phase. Here we have used single-molecule fluorescence resonance energy transfer (FRET) to reveal three phases of λ exonuclease reactions: the initiation, distributive and processive phases. The distributive phase comprises early reactions in which the 3′ overhang is too short to stably engage with the enzyme. A mismatched base is digested one-fifth as quickly as a Watson-Crick-paired base, and multiple concatenated mismatches have a cooperatively negative effect, highlighting the crucial role of base pairing in aligning the 5′ end toward the active site. The rate-limiting step during processive degradation seems to be the post-cleavage melting of the terminal base pair. We also found that an escape from a known pausing sequence requires enzyme backtracking.

DNA exonucleases catalyze numerous biological processes involved in DNA replication, recombination and repair[1]. Bacteriophage λ encodes a 5′-to-3′ exonuclease that creates an early DNA intermediate during initiation of homologous recombination[2]. The λ exonuclease preferentially recognizes the 5′-terminal phosphate in linear duplex DNA and processively degrades the strand with the phosphate in the 5′-to-3′ direction, producing a 3′ overhang tail of the nonhydrolyzed strand[3–6]. Annealing factors such as Redβ further process the product of the λ exonuclease reaction during homologous recombination[7], with or without the aid of host proteins such as RecA and SSB[8,9].

A ring-shaped structure is a recurring feature for many proteins involved with processive reactions on nucleic acid substrates[10]. Examples include λ exonuclease in DNA degradation; polynucleotide phosphorylase[11,12] and the exosome in RNA degradation; and hexameric helicases, PCNA and the β-clamp in DNA replication. Because the central channel forms a ring through which nucleic acid strands are believed to pass, the proteins do not easily fall off during reactions. Accordingly, λ exonuclease digests double-stranded DNA (dsDNA) highly processively (>3,000 nucleotides (nt) per attempt)[4,5] but cuts single-stranded DNA (ssDNA) inefficiently, in a distributive manner[13,14]. The translocation of λ exonuclease along DNA does not require ATP, but does require Mg^{2+} as a cofactor; it is fueled by the chemical energy released from the hydrolysis of the phosphodiester bond. The processive degradation rates have been measured as 10–12 nt s^{-1} by bulk biochemical studies[13,15] and 13–18 nt s^{-1} by single-molecule studies[16–18].

Many enzymatic activities are comprised of multiple distinct stages. For instance, RNA polymerase undergoes a transition from the initiation phase to the elongation phase during transcription[19]. The initiation phase is characterized by a high frequency of abortive synthesis of short transcripts, whereas the elongation phase comprises a rapid and highly processive RNA synthesis reaction. The ribosome also undergoes several mechanistically distinct phases during translation, including initiation, elongation and termination[20]. The initiation steps of DNA unwinding by the RecBCD helicase-nuclease complex have also been studied in detail[21–23]. However, nuclease activities have not been dissected in such fine detail. Typically, nuclease activities have only been classified as either distributive or processive.

Recent progress in single-molecule techniques has made it possible to detect rich dynamics of biological macromolecules, such as enzymatic dynamic disorder[18], heterogeneity[24–26], transient intermediates[27–29] and hidden complexity[30]. Here we have used single-molecule FRET[31,32] to dissect the dynamics of λ exonuclease. We found that the DNA-degradation reaction cycle of this enzyme includes three distinct phases.

RESULTS

Single-molecule fluorescence assay for λ exonuclease

λ exonuclease forms a homotrimeric ring structure with a tapered central channel (**Fig. 1a**,**b**). The diameter at the entrance of the channel is ~30 Å, wide enough to accommodate dsDNA (dotted orange ring, **Fig. 1a**), whereas the diameter at the exit is ~15 Å, narrow enough to sterically reject dsDNA, allowing only ssDNA to pass through (dotted red ring, **Fig. 1a**)[33]. This geometrical constraint creates an extrusion platform where dsDNA can enter but only ssDNA comes out. Here, for the sake of presentation, we will assume that the functional form of the enzyme is the trimeric ring, but it should be noted that there has not been direct demonstration of this widely held assumption.

To analyze the λ exonuclease activity with high resolution at the single-molecule level, we designed a blunt-ended dsDNA substrate in which a phosphate group is attached on the 5′ end of the hydrolyzed strand (termed the 5′ strand here). The FRET donor (Cy3) is conjugated to the 3′ end of the nonhydrolyzed strand (termed the 3′ strand), and the acceptor (Cy5) is conjugated to the same strand 20 nt away from the 3′ end (**Fig. 1c**). FRET between Cy3 and Cy5 can report on the reaction progress as follows. As the 5′ strand is degraded, the 3′ strand becomes single stranded and then coils up[34,35], decreasing the time-averaged distance between the fluorophores, which leads to an increase in FRET. The other end of the DNA, without 5′ phosphorylation, is tethered to a polymer-coated quartz surface via biotin-neutravidin interaction.

When reaction solution containing λ exonuclease and 2.5 mM $MgCl_2$ was added to the surface-tethered DNA molecules via a flow delivery system[36], digestion took place from the 5′ strand, with

[1]Department of Physics and the Center for the Physics of Living Cells, University of Illinois at Urbana-Champaign, Urbana, Illinois 61801, USA. [2]Howard Hughes Medical Institute, Urbana, Illinois 61801, USA. *e-mail: tjha@illinois.edu

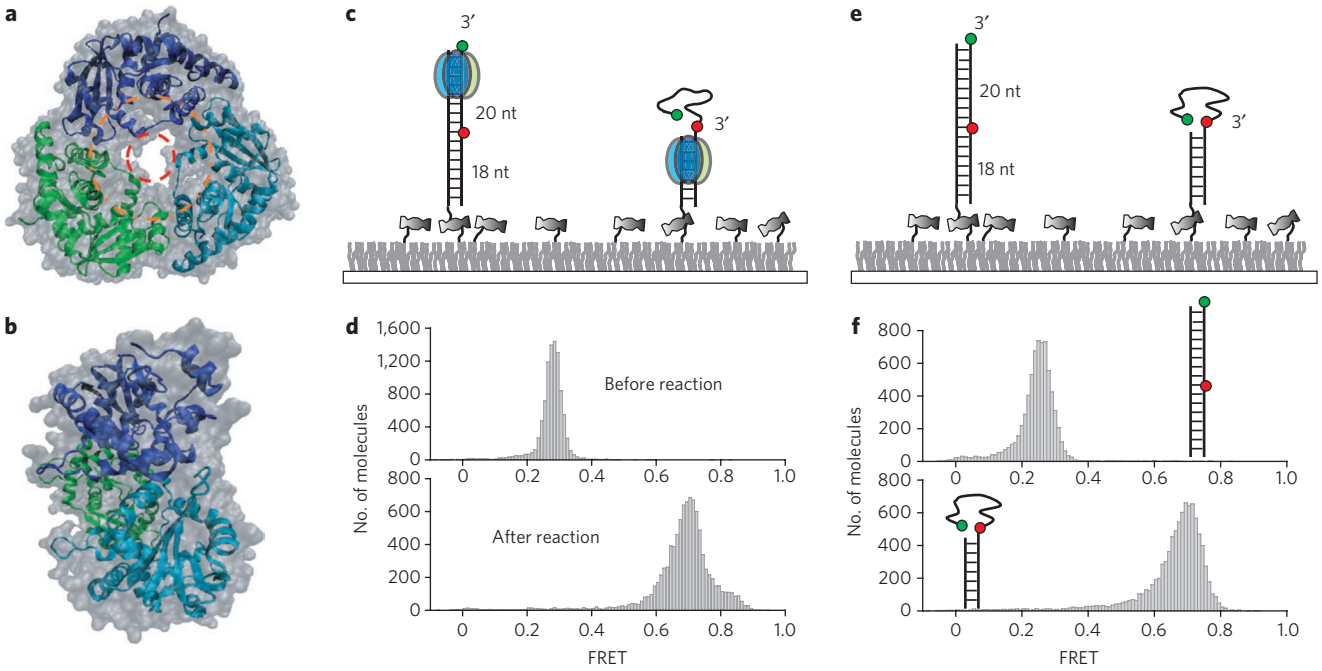

Figure 1 | Single-molecule FRET assay for λ exonuclease activity. (**a**) Top-to-bottom view of the crystal structure of λ exonuclease. dsDNA is thought to enter the outer ring, which is ~30 Å in diameter (orange), with ssDNA product exiting from the inner ring, ~15 Å in diameter. (**b**) Side view of the crystal structure, showing tapering from the entrance on the right to the exit on the left. (**c**) Schematics showing the experiment before (left) and after (right) degradation by λ exonuclease. The enzyme converts dsDNA between the donor (green) and the acceptor (red) to ssDNA, causing an increase in FRET. (**d**) Single-molecule FRET histograms before and after the degradation. (**e**) A partial duplex mimicking the degradation product was constructed to estimate the FRET value after the degradation. (**f**) Single-molecule FRET histograms built from dsDNA and partial duplex in the absence of λ exonuclease.

concomitant sliding of λ exonuclease along the 3′ strand. This process decreased the time-averaged distance between the two fluorophores by converting a rigid dsDNA into a flexible ssDNA (**Fig. 1c**). The single-molecule histogram of FRET efficiency E shifted from a peak at E = 0.27 before the reaction to a peak at E = 0.72 after the reaction (**Fig. 1d** and **Supplementary Fig. 1**). To check whether the E = 0.72 state resulted from the degradation product, we constructed a partial duplex that mimics the reaction product. We also found a peak at E = 0.72 from this control DNA only (**Fig. 1e**,**f**). This comparison demonstrates that the single-molecule FRET signal is a good measure of the DNA degradation reaction.

Protein concentration–dependent reaction phases

Figure 2a shows representative single-molecule time traces obtained from a single DNA molecule during degradation. The reaction buffer containing the protein and Mg^{2+} was introduced to the imaging chamber at the time indicated as 'injection'. Subsequently, a protein binding event was detected as fluorescence jumps in both donor and acceptor intensities owing to protein-induced fluorescence enhancement[37–39] (black, upper graph). Degradation was then observed as progressive increases in FRET (blue, lower graph) caused by a decrease in donor intensity (green, middle graph) together with an increase in acceptor intensity (red, middle graph). Consistent with the histograms showing that more than 90% of the DNA molecules were converted into ssDNA (**Fig. 1d**), the real-time single-molecule time traces showed evidence of DNA degradation for more than 90% of the DNA molecules.

To characterize the time traces in detail, we defined three different time periods (**Fig. 2a**): (i) the 'protein binding period', which begins when the reaction buffer is injected and ends when fluorescence intensities jump; (ii) the 'initiation period', during which enhanced fluorescence intensities are evident but FRET stays at a constant low level; and (iii) the 'degradation period', during which FRET increases from the minimum to the maximum values. We considered the initiation time to be the time from initial protein binding until the formation of a functional DNA–protein complex capable of the nuclease reaction.

We analyzed dwell times for all three periods as a function of protein concentration, ranging from 0.6 nM to 120 nM (monomer concentration; **Supplementary Figs. 2–5**). The protein binding period showed a dependence on protein concentration, as expected (top curve in **Fig. 2b**). Notably, the initiation period also showed protein-concentration dependence (middle curve in **Fig. 2b**). To date, it has not been demonstrated that the active form is the trimeric ring, and our method cannot directly probe the assembly state of the protein. Nevertheless, the data show that a single binding event of protein(s) is not enough to catalyze reactions that are detectable via FRET change. Both the rate of binding and the rate of initiation initially increased linearly with protein concentration, not sigmoidally, suggesting that these steps do not represent the assembly of a trimer from monomers in solution. The initiation time reached a plateau of about 1.6 s at saturating protein concentrations, substantially longer than the estimated timescale of protein delivery via flow (<0.4 s). Therefore, the initiation period probably involves a conformational change of the protein complex as well as protein binding.

Unexpectedly, the degradation period was also shortened with increasing protein concentration (bottom curve in **Fig. 2b**). Close examination of individual traces showed several pauses during the reaction (indicated by black arrows in **Fig. 2c**). In addition, the average pause dwell times were longer at lower protein concentrations (**Fig. 2d** and **Supplementary Table 1**). We infer that the reason the first 20 base pairs (bp) are degraded at a concentration-dependent overall speed is because the functional enzyme tends to dissociate, so that the reaction pauses until a functional enzyme unit rebinds. At present, we cannot determine whether the enzyme complex dissociates as a whole or only in part. The apparent saturation in the rate of reinitiating degradation at high protein concentrations (**Fig. 2d**) suggests that an additional step (other than protein binding) is

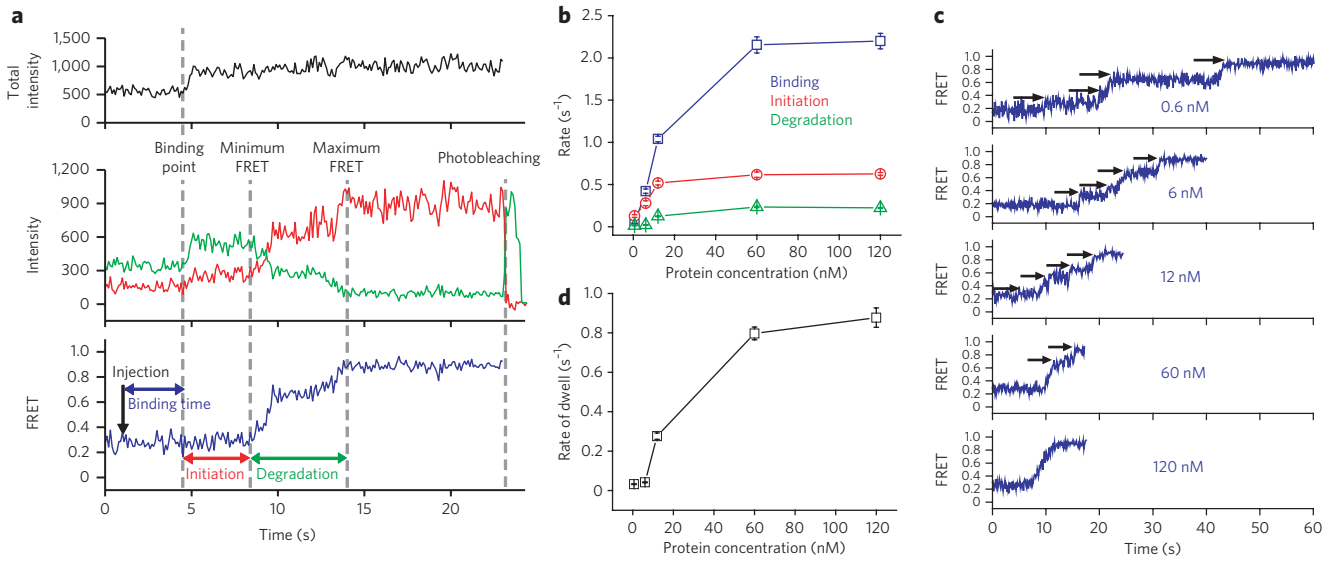

Figure 2 | λ exonuclease carries out initiation and distributive degradation until it is stably engaged by the substrate. (**a**) Schematic showing how binding time, initiation time and degradation time are assigned. The protein binding period begins when the reaction buffer is injected and ends right before the enhancement of both fluorescence intensities. During the initiation period, fluorescence intensities increase but FRET stays at a constant low level. In the degradation period, FRET increases from the minimum to the maximum values. Total intensity is the sum of the donor and acceptor intensities (black, top graph). Green and red curves represent the donor and acceptor intensities, respectively (middle graph), and the blue curve represents the calculated FRET efficiency (bottom graph). (**b**) Inverse of characteristic times of binding, initiation and degradation versus protein concentration. Each data point is an average of more than 200 molecules (see **Supplementary Figs. 2–4** for their distributions). (**c**) Representative single-molecule time traces for various protein concentrations. Below 60 nM protein, the time traces show multiple pauses, indicating frequent dissociation of λ exonuclease from the substrate. (**d**) Average pause duration versus protein concentration (see **Supplementary Fig. 5** for distributions). Error bars denote s.e.m.

required for the rescue to occur. This concentration-dependent behavior is characteristic of distributive enzymes, and we therefore did not expect it from the highly processive λ exonuclease. We postulated that λ exonuclease may perform distributive degradation events during initial degradation until the 3′ ssDNA overhang generated is of sufficient length to engage the enzyme stably. If so, our FRET-based assay should show processive degradation once the 3′ overhang becomes long enough. We tested this prediction next.

Protein concentration–independent reaction phase

We lengthened the upstream sequence of the original substrate by 23 bp, a longer distance than the enzyme footprint (~13–14 nt)[15], to monitor degradation after λ exonuclease is stably engaged by the 3′ strand. The reference FRET value measured in the absence of protein was ~0.27 for the extended construct and ~0.55 for the partial duplex mimicking the degradation product (**Fig. 3a**). FRET values of the substrate before the reaction (with λ exonuclease but without Mg^{2+}) and after the reaction (with λ exonuclease and Mg^{2+}) agreed with the reference FRET values (**Fig. 3b**), demonstrating that the extended construct is efficiently degraded by λ exonuclease under our experimental conditions. We also carried out a gel-based degradation assay to determine whether fluorophore labeling of the 3′ strand inhibits the degradation of the 5′ strand. The gel assay showed that the 3′ strand was efficiently degraded; the labeling had a minimal effect on the reaction (**Supplementary Fig. 6**).

The real-time single-molecule FRET time traces of the extended construct showed a gradual FRET increase that began 1–200 s after protein injection (**Fig. 3c** and **Supplementary Fig. 7**). The delay time between protein injection and commencement of degradation beyond the first 23 bp was protein concentration dependent (**Supplementary Fig. 7**). This was consistent with our proposal of distributive degradation activity on the first 20 bp, as we had earlier observed with the original construct. Therefore, the distributive activity on the original construct cannot be due to the terminal labeling of the 3′ strand with a fluorophore.

In contrast to the protein concentration–dependent delay time, the average reaction duration for degradation of the DNA segment from base pair 23 to base pair 43 was not dependent on protein concentration (**Fig. 3d**), indicating that FRET increase in the extended construct was reporting on the processive phase of the reaction. The degradation rate—the number of nucleotides degraded (20 nt) divided by the degradation time (1.1 s)—was ~18 nt s^{-1}, and this stayed constant over a wide range of protein concentrations, from 1.2 nM to 120 nM. This rate is at least fourfold faster than the concentration-dependent overall rates (~4.4 nt s^{-1} at maximum) during the distributive phase. We further tested whether we could recover the rate of processive degradation from the time traces of the distributive phase by removing the pauses (**Supplementary Fig. 8**). The overall reaction times showed very similar distributions once the pauses were removed. Therefore, the time spent in paused states accounts for most of the differences between the apparent reaction rates of the processive and distributive phases. Our observations provide experimental support for the proposal that the encircling of the trimeric ring around the ssDNA generated in the digestion is the reason for λ exonuclease's rapid and highly processive activity, because the processive phase does not begin until up to 23 nt of 3′ ssDNA overhang is generated.

Next we site-specifically labeled λ exonuclease at the N terminus with CoA-547 fluorophore, which is spectrally equivalent to Cy3, using Sfp phosphopantetheinyl transferase[40,41] (**Supplementary Methods**), with a labeling efficiency of 17%. We used this fluorescently labeled protein on the same extended construct used in the experiments of **Figure 3a**, with Cy3 and Cy5 labels designed to probe the processive phase. This combination allowed us to monitor protein binding and dissociation via signal changes in the Cy3 channel while at the same time observing the processive degradation via changes in FRET between the fluorophores on the DNA. As this measurement does not require the determination of absolute FRET efficiencies, we calculated the apparent FRET efficiencies as the acceptor intensity divided by

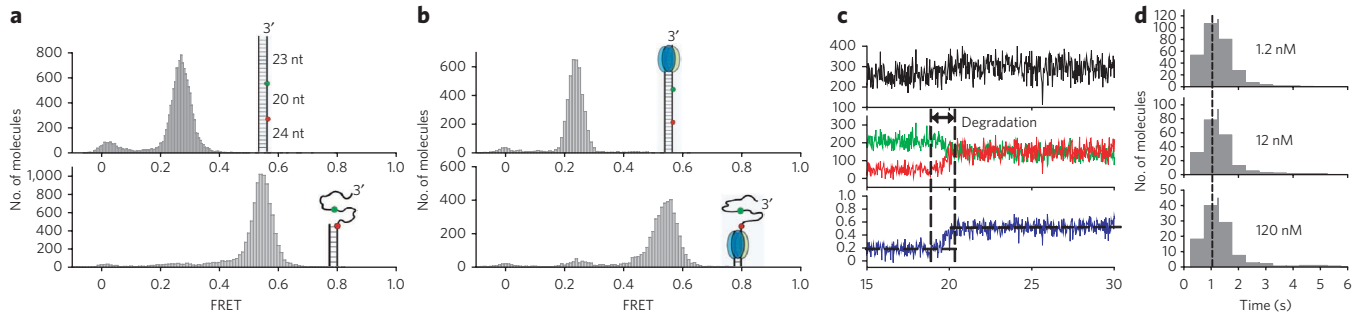

Figure 3 | After stable engagement with the 3′ overhang, λ exonuclease processively degrades the substrate without dissociating. (**a**) Single-molecule FRET histograms of an extended construct (top) and a partial duplex mimicking the reaction product (bottom) in the absence of the protein. Cartoons to right of histograms show the constructs. To detect DNA degradation after the protein is stably engaged with the substrate, we extended the original DNA construct used in **Figures 1** and **2** by 23 bp upstream of the FRET tags. The extension of 23 bp is longer than the footprint of the enzyme (13–14 nt), ensuring that the substrate can be fully engaged when the enzyme passes the region between two fluorophores. (**b**) Single-molecule FRET histograms obtained after λ exonuclease was injected into reaction chambers without Mg^{2+} (top) and with Mg^{2+} (bottom). Comparison of histograms in **a** and **b** verified that DNA degradation indeed occurred (indicated by cartoons). (**c**) A representative set of time traces from a single molecule of the extended construct during degradation (120 nM protein). The degradation period measured by FRET is marked. (**d**) Histograms of degradation times at different protein concentrations are identical to each other, showing that the FRET increase from the extended construct reports on the processive phase.

the sum of donor and acceptor intensities, regardless of whether there was more than one donor present or not.

We tested two different concentrations of the enzyme, 6 nM and 60 nM. In the Cy3 channel, we observed discrete intensity fluctuations between high and low values, probably owing to binding and dissociation of labeled proteins, until the processive degradation started (**Fig. 4a**,**b**). We measured the degradation time of the first 23 bp of the DNA as the time from the protein addition until FRET started to increase (marked by magenta arrows in **Fig. 4a**,**b**). The degradation time, which reflects the distributive phase, was shorter at the higher protein concentration (**Fig. 4c**). The frequency of binding events, in contrast, was greater at the higher protein concentration (**Fig. 4d**). The binding and unbinding events did not occur once the processive phase started (**Fig. 4a**,**b**), showing that the events we observed are specific to the distributive phase. In summary, the experiments using the labeled enzyme further support our model in which multiple binding and dissociation events occur in the distributive phase. Whether the binding and dissociating unit is a monomer or a trimer could not be determined, given the low labeling efficiency.

λ exonuclease carries out three phases of degradation. On the basis of our data, we can divide the degradation activity of λ exonuclease into three phases: the initiation phase, the distributive degradation phase and the processive degradation phase (**Fig. 4e**). Protein concentration affects both the rate of initiation and the rate of distributive degradation, whereas the rate of processive degradation is independent of protein concentration. The initiation phase is a process forming a catalytically functional DNA–protein complex, whereas the distributive degradation phase is an intermediate process through which the initiation phase transits to the processive phase, presumably via the enzyme encircling the 3′ ssDNA overhang that has been generated. Finally, processive degradation is a highly efficient process, during which thousands of nucleotides are digested without enzyme dissociation.

Base-pair mismatches slow degradation

Each catalytic cycle of λ exonuclease is composed of (i) hydrolytic scission of a phosphodiester bond, (ii) 5′-to-3′ translocation along DNA by 1 nt and (iii) melting of the next base pair at the junction between the 3′ ssDNA tail and the duplex. At present, it is unclear how these events are coordinated and temporally ordered. A previous study has found that the enzyme digests DNA regions that are rich in A-T base pairs faster than G-C–rich regions, suggesting that melting is rate limiting in the overall reaction[18]. This in turn suggests that the melting of duplex, presumably at the terminal base pair, is a prerequisite for the next round of the cleavage reaction. If so, introducing single–base pair mismatches into the duplex DNA might allow the enzyme to digest the DNA faster because the enzyme would not need to break base-pairing interactions. We examined the role of DNA base pairing in degradation. Five mismatches were introduced, one every 4 nt over the 20-nt distance between two fluorophores, in the extended construct that reports on the processive phase (5Ms in **Fig. 5a**). Contrary to our expectation, we found that the degradation of this sparsely mismatched construct was half as fast as the fully base-paired construct (~2 s overall reaction time, compared with ~1 s; **Figs. 3** and **5**, and **Supplementary Fig. 9**). As the presence of five isolated mismatches slowed down the reaction of the 20-bp region by 50%, we can also deduce that the reaction at a single-mismatch site is about one-fifth as fast as the reaction at an intact one (**Supplementary Fig. 10**). We further examined the effect of mismatches by introducing between two and five consecutive mismatches (2M to 5M in **Fig. 5a**). **Figure 5c** shows examples of time traces from single-molecule FRET. The average degradation time lengthened with increasing number of mismatches (**Fig. 5d**). Notably, the time increase was nonlinear (that is, faster than a linear increase), showing that the effect of sequential mismatches is synergistic. We suggest that base-pairing interactions stimulate DNA degradation by λ exonuclease, possibly by aligning the 5′ end of the degradation strand toward the active site of the protein. In addition, five sparse mismatches over a 20-bp region slowed down the reaction by 50%, whereas five consecutive mismatches slowed down the reaction by 71%. These results suggest that the helicity of the duplex is important for processive degradation by λ exonuclease.

A DNA bubble can arrest degradation

As a further test of the effect of mismatches, we designed a bubble construct with a stretch of 18 mismatches between the two fluorophores to see whether degradation would slow down further (**Supplementary Fig. 11**, bottom panel inset). **Figure 6a** shows single-molecule FRET efficiency histograms at different times in the reaction. The histogram for the undigested bubble DNA shows a FRET peak at $E = 0.33$, which is higher than the FRET at $E \approx 0.27$ measured from the fully base-paired DNA, probably because of the collapse of the ssDNA segment between the two fluorophores. The histogram obtained 2 min into the reaction shows a broad FRET distribution, ranging from 0.2 to 0.6, instead of the narrow FRET

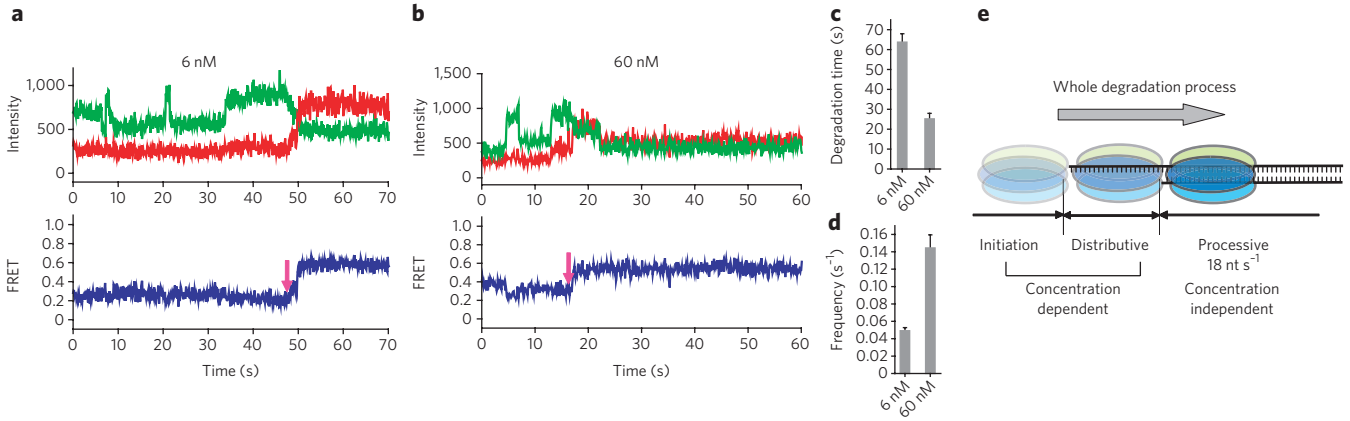

Figure 4 | λ exonuclease performs distributive degradation before complete engagement to DNA. (**a**,**b**) Representative single-molecule time traces of the acceptor and donor channel signals obtained with the extended construct (**Fig. 3**) in the presence of 6 nM (**a**) or 60 nM (**b**) CoA-547–labeled protein. Multiple increase and decrease events in the donor channel signal appear before FRET starts to increase upon degradation beyond the first 23 bp (magenta arrows). Note that the binding and unbinding events do not occur once the processive phase starts, showing that the events observed are specific to the distributive phase. (**c**) Average degradation time for the first 23 bp of the extended construct, determined from the time between protein addition and the moment that FRET starts to increase (magenta arrows in **a**,**b**). Error bars denote the s.e.m. (**d**) Average frequency of donor intensity increase and decrease events before FRET starts to increase. (**e**) Model of DNA degradation of λ exonuclease. The degradation activity of λ exonuclease is divided into three phases: initiation, distributive degradation and processive degradation.

peak at 0.55 observed from the standard substrate, suggesting that the bubble structure delays the degradation reaction by λ exonuclease (**Supplementary Fig. 11**). The histogram obtained 30 min after the start of the reaction shows that λ exonuclease is still captured or stalled in the bubble region at this time. This contrasts with the histogram obtained from a 2-min reaction of the full intact duplex substrate, which showed a narrow peak, indicating that the λ exonuclease passed through the labeled region and reached the downstream region of the substrate (**Fig. 3b**, lower graph). With the 18-mismatch substrate, when we washed out the proteins in solution by flushing the chamber with additional reaction buffer after 30 min, the major FRET peak shifted to high FRET owing to ssDNA collapse after λ exonuclease dissociation (**Fig. 6a**, bottom graph). These data overall suggest that the enzyme is unable to degrade the DNA through a large bubble.

When λ exonuclease encounters a mismatch or a bubble, the 5′ end of the degradation strand should become unconstrained (**Fig. 6b**), which may result in misalignment of the 5′ end with the active site of the enzyme owing to poor helicity caused by mismatches. In addition, the degradation end may fluctuate away from the active site so that λ exonuclease may not grab the 5′ end readily, whereas the 5′ end on the intact B-form helix is maintained in the correct orientation, which guides it to the active site. In the case of the bubble, a fork or 'Y' branch shape is created upon cleavage at the beginning of bubble, and the 5′ end might deviate completely out of the tapered engaging ring (**Fig. 6b**). The enzyme would thus be trapped on the 3′ strand for a long period of time, resulting in the arrest of degradation (**Fig. 6a**, third graph). We carried out a gel assay to confirm that a large bubble (20 nt) causes the arrest of degradation (**Supplementary Fig. 12**), consistent with the single-molecule data.

Escape from sequence-dependent pausing

We constructed a DNA containing the GGCGATTCT sequence to reproduce the pausing behavior of the enzyme originally reported in 2003 (ref. 17). We inserted the sequence in the middle of our duplex construct so that if there were a pause, it would show up during the processive phase of the reaction. Indeed, we observed a reproducible pause at FRET of $E \approx 0.4$ (**Fig. 6c**), and the pause time was

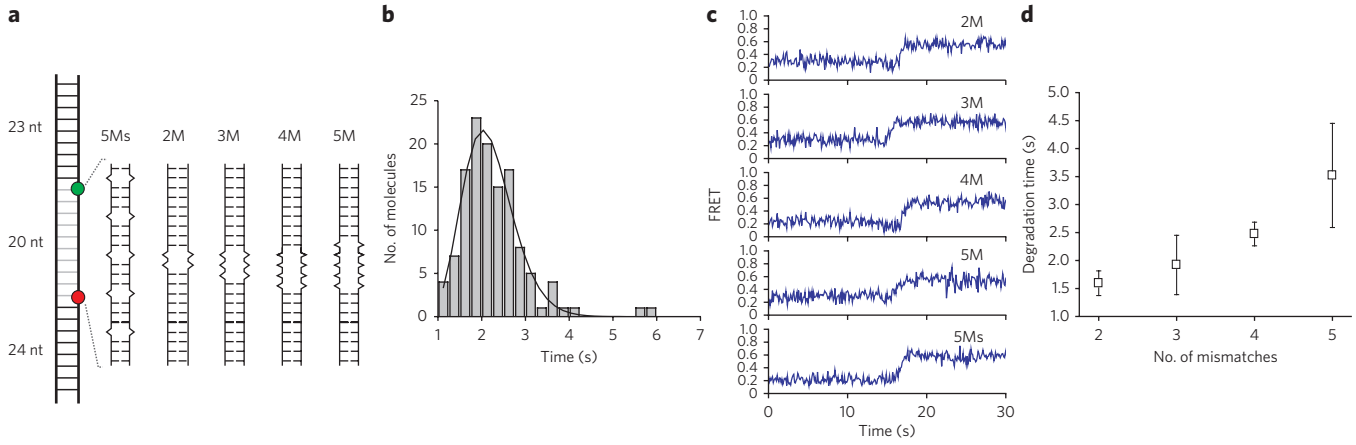

Figure 5 | DNA mismatches impede the degradation activity of λ exonuclease in a synergistic manner. (**a**) Schematics of DNA constructs with five periodic, sparse mismatches (5Ms) and with two to five consecutive mismatches (2M to 5M). (**b**) Histogram of degradation time for 5Ms DNA. (**c**) Representative single-molecule FRET time traces from mismatched DNA constructs in **a**. (**d**) Average degradation time as a function of the number of consecutive mismatches shows that the effect of mismatches is non-additive if they are concatenated. Error bars denote s.e.m.

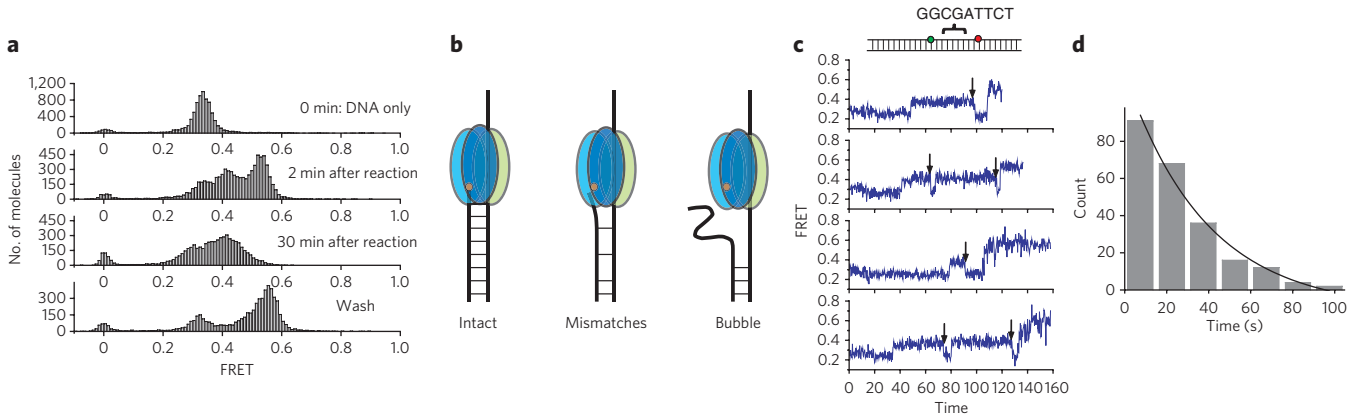

Figure 6 | Degradation arrest on a bubble DNA and escape from a known pausing sequence. (**a**) Single-molecule FRET histograms of a bubble DNA construct with 18 mismatches between the donor and the acceptor. Shown are results with DNA only, after 2-min or 30-min incubation with 120 nM protein, and upon washing after 30-min incubation. (**b**) Model of λ exonuclease degrading intact, mismatched and bubble DNAs. The bubble causes degradation arrest. The orange dot represents the active site of λ exonuclease. (**c**) Representative single-molecule FRET time traces during degradation of a DNA construct containing the known pausing sequence (cartoon at top) with 120 nM protein. After it pauses, λ exonuclease appears to backtrack (FRET decrease, black arrows) before continuing to degrade the DNA. (**d**) Histogram of pause duration and an exponential fit. The average pause duration is 24.2 ± 1.3 s (229 molecules).

24.2 ± 1.3 s on average (229 molecules; **Fig. 6d**). This experiment shed new light on how the enzyme can be rescued from the paused state. Before it progresses past the pause site, it often moves backwards, indicated by a drop in FRET (**Fig. 6c**, black arrows). Over 90% of observed molecules (230 of 248 molecules) showed backtracking before continued degradation. This backtracking, reminiscent of RNA polymerase backtracking[34], may be explained as follows.

When λ exonuclease digests DNA one nucleotide at a time, its precise registration of each nucleotide may allow the enzyme to recognize a particular DNA sequence that generates a strong interaction with the enzyme so that the enzyme stalls in a sequence-dependent manner[17]. In contrast, when λ exonuclease backtracks from the pause site, such a motion presumably occurs by diffusion because there is no DNA hydrolysis involved in the backward movement. During the diffusion, the enzyme may not register every single nucleotide, allowing it to bypass the pausing sequence. The average lifetime of the paused state is about 50% shorter in optical-tweezers experiments[17]; one possible explanation is that application of ~1 pN of force may aid backtracking on ssDNA, required for escape from the paused state. Backward movements were observed very infrequently in the processive mode of our standard sequence (1 of 532 traces; see, for example, **Supplementary Fig. 13**).

DISCUSSION

We have developed a single-molecule FRET assay that allows us to monitor the real-time enzymatic action of individual functional units of λ exonuclease. Different DNA substrates were designed to have high sensitivity in different stages of the reaction. We found that the DNA-degradation cycle of λ exonuclease comprises three reaction phases: an initiation phase and both distributive and processive degradation phases. Our findings offer a new way of conceptualizing the molecular basis for processive enzymes. For example, the mechanism by which proteins form catalytically competent complexes with DNA[22,37] has long been a topic of interest, but ensemble averaging in bulk studies can mask the detailed steps (see **Supplementary Fig. 14**). Our single-molecule assay bypasses the limitation of ensemble averaging and shows that the initiation phase that begins with the first protein binding event is also dependent on protein concentration (**Fig. 2b**). With direct readout of the initiation process, future studies may be able to reveal how enzyme mutations—for example, at the trimeric interfaces and putative DNA binding sites—affect the initiation process.

This study also found an additional distributive phase between initiation and processive degradation. The distributive process is characterized by frequent dissociation from the substrate. λ exonuclease carries out multiple rounds of short DNA-degradation events punctuated by enzyme dissociation and reassociation. The distributive phase might be biologically important, acting as a lag phase that allows the processive enzyme to interact with other viral factors such as Redβ (ref. 9) and Redγ, and host proteins such as RecA and SSB, to regulate the degradation reaction. Similarly, the abortive transcription of RNA polymerase has also been proposed as a potential point of regulation[42,43].

Mismatches and bubbles are lesions that frequently occur in the cell, and here we have used the high spatiotemporal resolution of our assay to investigate how they affect the processive phase of degradation. We found that multiple mismatches slow down the processive degradation rate of λ exonuclease in a non-additive manner. Fluctuations of the 5′ end liberated from the base pairing of the helix serve as a barrier so that λ exonuclease takes longer to form the functional DNA–protein complex acting on the 5′-phosphorylated end. These findings underscore the importance of 5′ end recognition for efficient resection.

How can our observation that a pre-melted duplex caused by mismatches delays degradation be reconciled with the previous finding that the G-C–rich region of the DNA substrate is degraded more slowly than the A-T–rich region[18]? The terminal base pair may remain intact until the hydrolytic scission and then melt to allow the release of the single-nucleotide product. If the melting of the terminal base pair is slower for G-C–rich regions even after the cleavage reaction, the two results can be reconciled by a reaction cycle with the following order: scission → base-pair melting → nucleotide release → 5′-to-3′ translocation. Although the duplex is pre-melted via mismatches ahead of the reaction cycle, the completion of the degradation cycle will slow down if scission is retarded by the deviation of the more flexible mismatched 5′ end from a catalytically competent complex. For the degradation of the intact duplex, our data and the results from a previous report[18] in combination suggest that the rate-limiting step is the post-cleavage melting of the terminal base pair.

METHODS

Protein and DNA. λ exonuclease was purchased from New England Biolabs (catalog no. M0262S) for DNA-labeled experiments. The protein used for the

protein-labeled experiment in **Figure 4** was expressed and purified as described in the **Supplementary Methods**. All DNA oligonucleotides were purchased from Integrated DNA Technologies. Biotin was conjugated at either the 5′ end of the 3′ strand (original construct, used in **Figs. 1** and **2**) or the 3′ end of the 5′ degradation strand (extended construct, used in **Fig. 3**). Both Cy3 and Cy5 were incorporated into the 3′ DNA strand via an internal modification during DNA synthesis by Integrated DNA Technologies (iCy3 and iCy5). Sequences of DNA and positions of biotin and fluorophores are provided in the **Supplementary Methods**.

Experimental conditions. DNA constructs were immobilized on a quartz surface coated with PEG (Laysan Bio) as shown in **Figures 1** and **3** to minimize nonspecific surface adsorption of proteins[44,45]. Immobilization was achieved via a specific molecular interaction between neutravidin (Pierce) and biotin moieties at the ends of DNA and biotin-modified PEG on the surface. We added 50–100 pM DNA molecules to the imaging chamber to obtain an appropriate density for single-molecule imaging. Glucose and glucose oxidase were added to remove oxygen, which causes rapid photobleaching of fluorescent dyes. The reaction buffer contained 67 mM glycine-KOH (pH 9.4), 2.5 mM $MgCl_2$, 50 μg ml^{-1} BSA, 1 mg ml^{-1} Trolox[46] (Sigma-Aldrich) and an oxygen-scavenging system of 1mg ml^{-1} glucose oxidase (Sigma-Aldrich), 0.04% mg ml^{-1} catalase (Sigma-Aldrich) and 0.4% (w/v) D-glucose (Sigma-Aldrich). We constructed a flow chamber by assembling a microscope slide and a coverslip together with 3M double-sided tape and sealing with epoxy[36,47]. The holes on the slide were used for the inlet and outlet of solution exchange[36]. A 1-ml syringe was connected to the flow chamber through tubing, and a pipette tip that contained a reaction solution was tightly plugged into an inlet hole, preventing buffer leakage. When the syringe was pulled, the solution was introduced into the chamber at the rate of ~10 μl s^{-1}. The degradation reaction was started by injection of the reaction buffer containing λ exonuclease into an imaging chamber at room temperature.

Single-molecule data acquisition. Total internal reflection fluorescence microscopy was used to excite a FRET donor (Cy3) on the DNA with an Nd:YAG laser (532 nm, 75 mW, Crystal Laser). The fluorescence emission light from Cy3 and Cy5 was collected by a water-immersion objective lens (UPlanApo 60×, Olympus) and then sent through a 550-nm long-pass filter[48]. The fluorescence emission light was further separated into donor and acceptor signals with a 630-nm dichroic mirror (Chroma) and was detected by back-illuminated electron-multiplying charge-coupled device (EMCCD, Andor) with a time resolution of 30 or 100 ms. Fluorescence signals of donor and acceptor were amplified before camera readout. Thus, recorded fluorescence intensities of both Cy3 and Cy5 are in arbitrary units. The data were recorded in a video file format by an in-house software written in Visual C++. Single-molecule intensities were extracted from the recorded video file by IDL software, and FRET efficiency was calculated as the ratio of intensities, $\text{intensity}_{\text{acceptor}}/(\text{intensity}_{\text{donor}} + \text{intensity}_{\text{acceptor}})$, after we corrected for cross-talk between the donor and acceptor channels. All data were analyzed with programs written in MATLAB and plotted in Origin.

Received 6 May 2010; accepted 25 February 2011; published online 8 May 2011

References

1. Ceska, T.A. & Sayers, J.R. Structure-specific DNA cleavage by 5′ nucleases. *Trends Biochem. Sci.* **23**, 331–336 (1998).
2. Haber, J.E. In-vivo biochemistry: physical monitoring of recombination induced by site-specific endonucleases. *Bioessays* **17**, 609–620 (1995).
3. Little, J.W., Lehman, I.R. & Kaiser, A.D. An exonuclease induced by bacteriophage λ. I. Preparation of crystalline enzyme. *J. Biol. Chem.* **242**, 672–678 (1967).
4. Little, J.W. An exonuclease induced by bacteriophage λ. II. Nature of enzymatic reaction. *J. Biol. Chem.* **242**, 679–686 (1967).
5. Carter, D.M. & Radding, C.M. Role of exonuclease and β protein of phage λ in genetic recombination. II. Substrate specificity and mode of action of λ exonuclease. *J. Biol. Chem.* **246**, 2502–2512 (1971).
6. Thomas, K.R. & Olivera, B.M. Processivity of DNA exo-nucleases. *J. Biol. Chem.* **253**, 424–429 (1978).
7. Radding, C.M. Regulation of lambda exonuclease. I. Properties of lambda exonuclease purified from lysogens of lambda T11 and wild type. *J. Mol. Biol.* **18**, 235–250 (1966).
8. Black, L.W. DNA packaging in dsDNA bacteriophages. *Annu. Rev. Microbiol.* **43**, 267–292 (1989).
9. Muyrers, J.P.P., Zhang, Y.M., Buchholz, F. & Stewart, A.F. RecE/RecT and Redα/Redβ initiate double-stranded break repair by specifically interacting with their respective partners. *Genes Dev.* **14**, 1971–1982 (2000).
10. Hingorani, M.M. & O'Donnell, M. Toroidal proteins: running rings around DNA. *Curr. Biol.* **8**, R83–R86 (1998).
11. Guissani, A. Processive and synchronous mechanism of polynucleotide phosphorylase phosphorolysis: a comparison between experimental results and those calculated from a theoretical-study. *Eur. J. Biochem.* **79**, 233–243 (1977).
12. Klee, C.B. & Singer, M.F. Processive degradation of individual polyribonucleotide chains. II. *Micrococcus lysodeikticus* polynucleotide phosphorylase. *J. Biol. Chem.* **243**, 923–927 (1968).
13. Subramanian, K., Rutvisuttinunt, W., Scott, W. & Myers, R.S. The enzymatic basis of processivity in λ exonuclease. *Nucleic Acids Res.* **31**, 1585–1596 (2003).
14. Sriprakash, K.S., Lundh, N., Mooonhuh, M. & Radding, C.M. Specificity of λ exonuclease: interactions with single-stranded DNA. *J. Biol. Chem.* **250**, 5438–5445 (1975).
15. Mitsis, P.G. & Kwagh, J.G. Characterization of the interaction of lambda exonuclease with the ends of DNA. *Nucleic Acids Res.* **27**, 3057–3063 (1999).
16. Dapprich, J. Single-molecule DNA digestion by lambda-exonuclease. *Cytometry* **36**, 163–168 (1999).
17. Perkins, T.T., Dalal, R.V., Mitsis, P.G. & Block, S.M. Sequence-dependent pausing of single lambda exonuclease molecules. *Science* **301**, 1914–1918 (2003).
18. van Oijen, A.M. *et al.* Single-molecule kinetics of lambda exonuclease reveal base dependence and dynamic disorder. *Science* **301**, 1235–1238 (2003).
19. Young, B.A., Gruber, T.M. & Gross, C.A. Views of transcription initiation. *Cell* **109**, 417–420 (2002).
20. Marshall, R.A., Aitken, C.E., Dorywalska, M. & Puglisi, J.D. Translation at the single-molecule level. *Annu. Rev. Biochem.* **77**, 177–203 (2008).
21. Lucius, A.L., Wong, C.J. & Lohman, T.M. Fluorescence stopped-flow studies of single turnover kinetics of *E. coli* RecBCD helicase-catalyzed DNA unwinding. *J. Mol. Biol.* **339**, 731–750 (2004).
22. Wong, C.J., Lucius, A.L. & Lohman, T.M. Energetics of DNA end binding by *E. coli* RecBC and RecBCD helicases indicate loop formation in the 3′-single-stranded DNA tail. *J. Mol. Biol.* **352**, 765–782 (2005).
23. Wong, C.J., Rice, R.L., Baker, N.A., Ju, T. & Lohman, T.M. Probing 3′-ssDNA loop formation in *E. coli* RecBCD/RecBC-DNA complexes using non-natural DNA: a model for "Chi" recognition complexes. *J. Mol. Biol.* **362**, 26–43 (2006).
24. Zhuang, X. *et al.* A single-molecule study of RNA catalysis and folding. *Science* **288**, 2048–2051 (2000).
25. Zhuang, X. *et al.* Correlating structural dynamics and function in single ribozyme molecules. *Science* **296**, 1473–1476 (2002).
26. Rothwell, P.J. *et al.* Multiparameter single-molecule fluorescence spectroscopy reveals heterogeneity of HIV-1 reverse transcriptase: primer/template complexes. *Proc. Natl. Acad. Sci. USA* **100**, 1655–1660 (2003).
27. Hohng, S. *et al.* Fluorescence-force spectroscopy maps two-dimensional reaction landscape of the Holliday junction. *Science* **318**, 279–283 (2007).
28. Cecconi, C., Shank, E.A., Bustamante, C. & Marqusee, S. Direct observation of the three-state folding of a single protein molecule. *Science* **309**, 2057–2060 (2005).
29. Woodside, M.T. *et al.* Direct measurement of the full, sequence-dependent folding landscape of a nucleic acid. *Science* **314**, 1001–1004 (2006).
30. Shi, J., Dertouzos, J., Gafni, A., Steel, D. & Palfey, B.A. Single-molecule kinetics reveals signatures of half-sites reactivity in dihydroorotate dehydrogenase A catalysis. *Proc. Natl. Acad. Sci. USA* **103**, 5775–5780 (2006).
31. Stryer, L. & Haugland, R.P. Energy transfer: a spectroscopic ruler. *Proc. Natl. Acad. Sci. USA* **58**, 719–726 (1967).
32. Ha, T. *et al.* Probing the interaction between two single molecules: fluorescence resonance energy transfer between a single donor and a single acceptor. *Proc. Natl. Acad. Sci. USA* **93**, 6264–6268 (1996).
33. Kovall, R. & Matthews, B.W. Toroidal structure of lambda-exonuclease. *Science* **277**, 1824–1827 (1997).
34. Shaevitz, J.W., Abbondanzieri, E.A., Landick, R. & Block, S.M. Backtracking by single RNA polymerase molecules observed at near-base-pair resolution. *Nature* **426**, 684–687 (2003).
35. Murphy, M.C., Rasnik, I., Cheng, W., Lohman, T.M. & Ha, T.J. Probing single-stranded DNA conformational flexibility using fluorescence spectroscopy. *Biophys. J.* **86**, 2530–2537 (2004).
36. Selvin, P. & Ha, T. *Single-Molecule Techniques: A Laboratory Manual* 1st edn. (eds. Selvin, P.R. & Ha, T.) 3–36 (Cold Spring Harbor Laboratory Press, Cold Spring Harbor, New York, USA, 2008).
37. Maluf, N.K., Fischer, C.J. & Lohman, T.M. A dimer of *Escherichia coli* UvrD is the active form of the helicase in vitro. *J. Mol. Biol.* **325**, 913–935 (2003).
38. Luo, G., Wang, M., Konigsberg, W.H. & Xie, X.S. Single-molecule and ensemble fluorescence assays for a functionally important conformational change in T7 DNA polymerase. *Proc. Natl. Acad. Sci. USA* **104**, 12610–12615 (2007).
39. Myong, S. *et al.* Cytosolic viral sensor RIG-I is a 5′-triphosphate-dependent translocase on double-stranded RNA. *Science* **323**, 1070–1074 (2009).
40. Yin, J. *et al.* Single-cell FRET imaging of transferrin receptor trafficking dynamics by Sfp-catalyzed, site-specific protein labeling. *Chem. Biol.* **12**, 999–1006 (2005).
41. Yin, J., Lin, A.J., Golan, D.E. & Walsh, C.T. Site-specific protein labeling by Sfp phosphopantetheinyl transferase. *Nat. Protoc.* **1**, 280–285 (2006).

42. Hsu, L.M. Promoter clearance and escape in prokaryotes. *Biochim. Biophys. Acta* **1577**, 191–207 (2002).
43. Roberts, J.W. RNA polymerase, a scrunching machine. *Science* **314**, 1097–1098 (2006).
44. Ha, T. *et al.* Initiation and re-initiation of DNA unwinding by the *Escherichia coli* Rep helicase. *Nature* **419**, 638–641 (2002).
45. Roy, R., Hohng, S. & Ha, T. A practical guide to single-molecule FRET. *Nat. Methods* **5**, 507–516 (2008).
46. Rasnik, I., McKinney, S.A. & Ha, T. Nonblinking and longlasting single-molecule fluorescence imaging. *Nat. Methods* **3**, 891–893 (2006).
47. Grossman, D. & van Hoof, A. RNase II structure completes group portrait of 3′ exoribonucleases. *Nat. Struct. Mol. Biol.* **13**, 760–761 (2006).
48. Ha, T. Single-molecule fluorescence resonance energy transfer. *Methods* **25**, 78–86 (2001).

Acknowledgments

We thank R. Roy and X. Shi for experimental help, and J. Park for helpful discussions. G.L. was supported by the Jane Coffin Childs Medical Institute. Funds were provided by grants from the US National Science Foundation (0646550, 0822613) and the US National Institutes of Health (GM065367). T.H. is an investigator with the Howard Hughes Medical Institute.

Author contributions

G.L. performed single-molecule and ensemble fluorescent experiments. J.Y. performed single-molecule experiments. G.L. and B.J.L. expressed and purified λ exonuclease, and B.J.L. carried out the protein labeling. G.L., J.Y., B.J.L. and T.H. designed the experiments, analyzed the data and wrote the manuscript.

Competing financial interests

The authors declare no competing financial interests.

Additional information

Supplementary information is available online at http://www.nature.com/naturechemicalbiology/. Reprints and permissions information is available online at http://npg.nature.com/reprintsandpermissions/. Correspondence and requests for materials should be addressed to T.H.